

## Real time monitoring of relative velocity changes using ambient seismic noise at the Piton de la Fournaise volcano (La Réunion) from January 2006 to June 2007

Zacharie Duputel<sup>a,b,\*</sup>, Valérie Ferrazzini<sup>a,c</sup>, Florent Brenguier<sup>c</sup>, Nikolai Shapiro<sup>c</sup>, Michel Campillo<sup>d</sup>, Alexandre Nercessian<sup>c</sup>

<sup>a</sup> Observatoire Volcanologique du Piton de la Fournaise, 14 RN3 - Km 27, 97418 La Plaine des Cafres, Ile de La Réunion, France

<sup>b</sup> Institut de Physique du Globe de Strasbourg, 5 rue René Descartes, F-67084 Strasbourg cedex, France

<sup>c</sup> Institut de Physique du Globe de Paris, 4 place Jussieu, 75252 Paris cedex 05, France

<sup>d</sup> Laboratoire de Géophysique Interne et de Tectonophysique, BP 53, 38041 Grenoble CEDEX 9, France

### ARTICLE INFO

#### Article history:

Received 30 March 2008

Accepted 13 November 2008

Available online 3 December 2008

#### Keywords:

volcano monitoring  
ambient seismic noise  
seismic velocity variation  
caldera collapse

### ABSTRACT

We present the results of a real time method based on coda-wave interferometry from seismic noise cross-correlation functions for relative seismic velocity variations monitoring on a volcanic edifice. The ambient seismic noise at the Piton de la Fournaise volcano on La Réunion island is analyzed from January 2006 to June 2007. During this period, five eruptions occurred showing a great diversity in eruption duration, intensity and eruptive fissure location. Two different methods are used to compute the velocity variations in order to compare their stability in quasi real-time routine. We compare the obtained velocity variations with the surface deformation observed by GPS and extensometers networks. This allows us to identify and quantify three major processes at the origin of seismic wave velocity variations in the edifice. Firstly, the observed pre-eruptive summit inflation is accompanied by a decrease in seismic velocity. Secondly, the edifice deflation following the opening of an eruptive fissure is characterized by an increase of the velocity. Finally, the summit caldera collapse generates a strong velocity drop. Coda-wave interferometry from seismic noise cross-correlation functions in quasi-real time may allow us to forecast eruption and constrain the processes taking place in the volcanic plumbing system.

© 2008 Elsevier B.V. All rights reserved.

### 1. Introduction

Volcanic eruptions at the Piton de la Fournaise (PdF) are associated with permanent or transitory changes of the edifice elastic properties. These variations are revealed by an increase in seismicity, by the opening of fractures visible at the surface and by inflation–deflation cycles that affect the central cone (Aki and Ferrazzini, 2000; Peltier et al., 2006). The April 2007 major collapse involving the whole PdF summit highlights how important such changes can be on a volcanic edifice. The coda part of an earthquake is extremely sensitive to the propagation medium properties as the corresponding waves repeatedly sample the same region in space (Aki, 1985; Sato and Fehler, 1998). Jin and Aki (1986) exploit this high sensitivity, reporting a temporal change in the coda-attenuation factor,  $Q_c^{-1}$ , associated with the occurrence of the Tangshan earthquake ( $M_s = 7.8$ , 1976). However, their approach totally disregards the phase information. Another method proposed by Poupinet et al. (1984) and applied to Mt. Merapi by Ratdomopurbo and Poupinet (1995) takes advantage of the phase as well as the amplitude. After Snieder et al. (2002) and Snieder (2006),

this technique was named coda wave interferometry and applied to volcanoes by Grêt et al. (2005). The major drawback of using coda wave interferometry as a permanent survey method on PdF is the limited number, magnitude and localization of earthquakes between eruptions due to the region's low tectonic activity.

Nowadays, volcano monitoring is taking a new turn by combining passive imaging and coda wave interferometry techniques. Shapiro and Campillo (2004) and Roux et al. (2005) have shown that the Rayleigh wave Green's function (GF) between two receivers can be retrieved by cross-correlating long sequences of seismic noise. Brenguier et al. (2007) presented a 3D surface wave tomography of PdF using Rayleigh waves reconstructed from the cross-correlation over 18 months from 1999 to 2000 of ambient seismic noise. The resulting high resolution contrasts with previous tomographic studies that suffered from a poor distribution of the seismic sources, which were restricted above sea level under the central cone (Nercessian et al., 1996). This inversion shows a high velocity anomaly that confirms the presence of rift zones deeply anchored in the edifice. It also highlights an intrusive complex at shallow depth on the Northeastern flank of the central cone.

The wave field reconstructed from the ambient seismic noise can be used to detect small velocity changes in the propagation medium (Sens-Schönfelder and Wegler, 2006; Wegler and Sens-Schönfelder,

\* Corresponding author. Institut de Physique du Globe de Strasbourg, 5 rue René Descartes, F-67084 Strasbourg cedex, France. Tel.: +33 3 90 24 00 70.

E-mail address: [zacharie.duputel@eost.u-strasbg.fr](mailto:zacharie.duputel@eost.u-strasbg.fr) (Z. Duputel).

2007). Brenguier et al. (2008), using continuous data recording have shown that coda wave interferometry from ambient seismic noise could help forecast volcanic eruptions at the PdF. In the continuity of these works, the purpose of this paper is to present the real-time method developed at the Piton de la Fournaise Volcano Observatory to detect velocity variations in the edifice. After describing data processing and inversion, we will discuss the temporal variations associated with the 2006 eruptions and with the collapse of the entire Dolomieu crater during the major April 2007 eruption. Finally, we will compare the results to extensometer data and GPS ground displacements presented by Peltier et al. (2009-this issue).

## 2. Data processing

The PdF seismic network is essentially composed of 20 short period radiotelemetred seismometers (Mark Products L4C 1 Hz). Seismic data has been continuously recorded since 1999 allowing us to work on ambient seismic noise recordings. This study uses the vertical component signals of 15 seismic stations located in the Enclos Fouqué Caldera or in its immediate surrounding (Fig. 1).

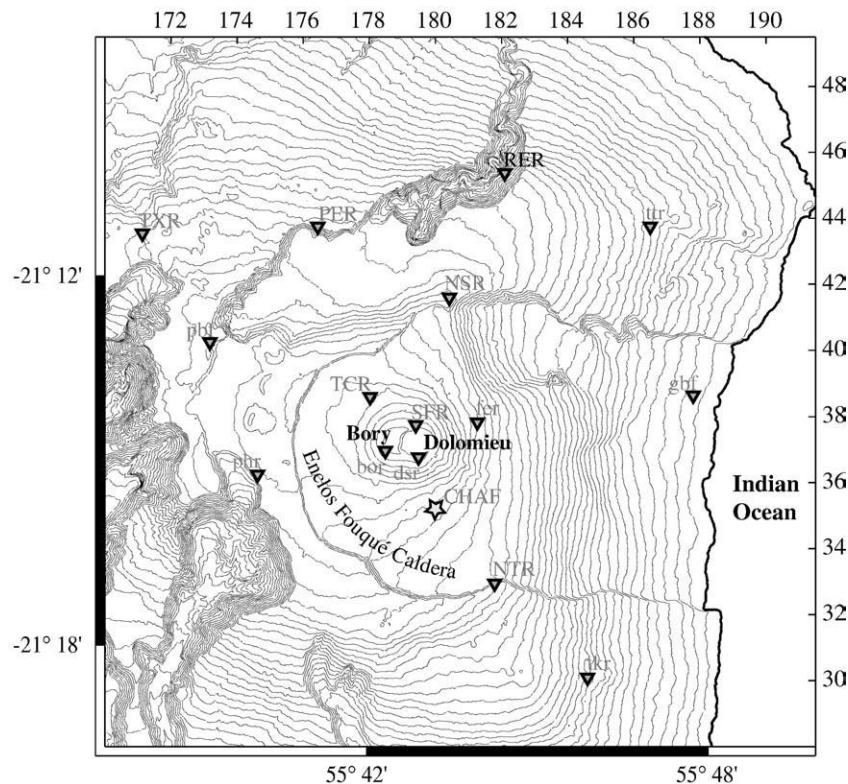
### 2.1. Green's function retrieval in real time

Every minute, SAC (seismic analysis code; Goldstein et al., 1998) data files of the 2 preceding minutes are produced by the Earthworm program (Johnson et al., 1995) in order to compute the cross-correlation for all data points for each pair of stations. Data processing essentially follows the approach used by Brenguier et al. (2008). After removing the mean and the trend from the signal, a spectral whitening and a one-bit normalization is applied. The cross-correlation function (CF) is then computed between signals of all possible pairs of stations. In order to obtain a one day averaged CF, after a first stack over 3 h, all the CF with a relatively low coherent amplitude are rejected. The retrieved

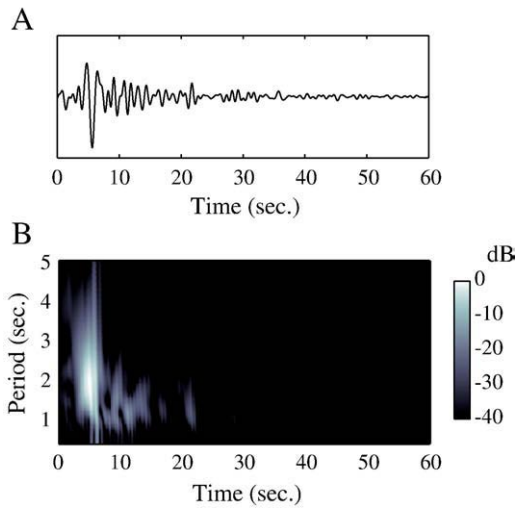
GF corresponds to the time derivative of the CF. Therefore, it differs only from the CF by a phase shift and a frequency proportional factor. Since the aim of the method is to detect velocity variations in the reconstructed waveform, it is unnecessary to compute the time derivative of the CF which would enhance high frequencies and may introduce spurious noise (Sabra et al., 2005).

Fig. 2 shows a frequency–time analysis of the CF for station pair “fer–pbr”. The spectrogram is dominated by the first arrivals with low frequencies corresponding to the direct Rayleigh wave between the two stations (Brenguier et al., 2007). As shown on Fig. 3C, these ballistic waves show a clear asymmetry between the causal and the anticausal part of the CF. This asymmetry reflects an inhomogeneous distribution of sources. The Rayleigh wave can be reasonably considered as due to the interaction between ocean swells at the nearest coastline, the so-called second microseismic peak around 5 s period in the ambient seismic noise (Aki and Richards, 2002; Stehly et al., 2006). The later arrivals have a higher frequency content (greater than 0.5 Hz). They often show phases with a good symmetry between causal and anticausal part of the CF (Fig. 3C) and are assumed to correspond to the scattered wavefield between the 2 stations used. The higher frequency content of this scattered wavefield may be due to the greater sensitivity of short wavelengths to small contrasts in the propagating medium. The symmetry in the coda is enhanced by multiple scattering that reduces the effect of local sources.

In order to detect temporal velocity variations in the medium, we need to compare the “current” CF with a reference CF. Fig. 4 shows the correlation coefficients between a reference CF averaged from April to July 2006 and a CF averaged over an increasing number of days for different frequency bands. A good coherency is reached most rapidly for the 0.5 to 1 Hz frequency band. The lack of coherency in the 0.2 to 0.7 Hz frequency band may be due to the instrument response of L4 geophones below 0.5 Hz. On the other hand, the bad reconstruction of the GF between 0.8 and 1.3 Hz can be explained by the lack of seismic



**Fig. 1.** Topography map of the PdF showing the seismic network around the Enclos Fouqué caldera (triangles). Bottom and left axes correspond to geographic coordinates. Top and right axes correspond to the Gauss Laborde coordinates in kilometers (origin at 21.5°S, 54.0°E). Lowercase letters correspond to numerical stations whereas analogical seismic stations are in uppercase. The extensometer station named “CHAF” is also indicated by a star.



**Fig. 2.** Spectral content of the correlation function for station pair “fer-pbr”. (A), Cross-correlation function after averaging the causal and the anticausal part. (B), Corresponding wavelet-based time-frequency analysis (using a Morlet wavelet).

sources in this band. Thus we choose to compute the “current” CF using 10 days averaged CF and the reference CF using at least two months averaged CF. The resulting CF are then filtered between 0.5 and 1 Hz before estimating the temporal velocity variation. This frequency band also highlights the scattered wavefield (Fig. 2) and minimizes the effects of eruption tremors which have dominant frequencies usually ranging between 2 Hz and 4 Hz.

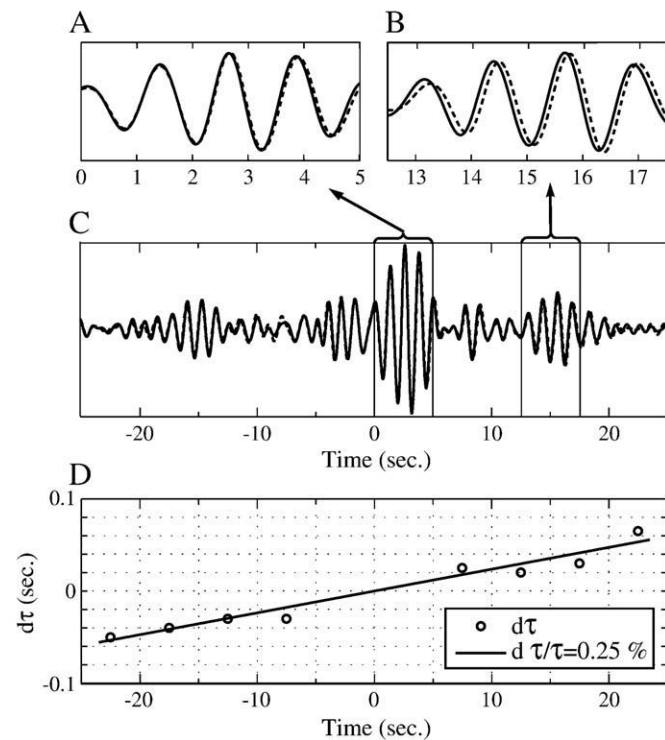


**Fig. 3.** Temporal variation for station pair “fer-dsr” associated with the July 2006 eruption. Details of the cross-correlation function (C) showing in (A) the ballistic waves and (B) the scattered waves. The reference correlation function is shown as a plain line whereas the cross-correlation function averaged within the 10 days preceding the eruption is represented as a dotted line. (D),  $d\tau$  (circles) deduced from cross-correlation between the reference correlation function and the one averaged over the 10 days before fracture opening. The linear regression of method 1 is shown as a straight line and corresponds to  $d\tau/\tau = 0.24\%$ .

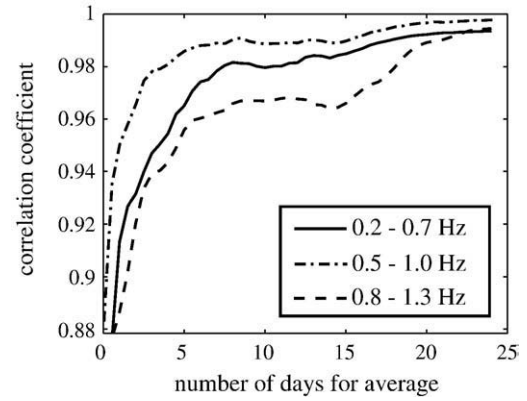


**Fig. 4.** Correlation coefficient considering different frequency bands and using an increasing number of days for the cross-correlation function average. This was computed during May 2006 for station pair fer-bor assuming a reference CF averaged from April to July 2006.

## 2.2. Relative velocity variations estimation method

The next step is to estimate the relative velocity variations in the medium. Let us consider a relative velocity variation  $dv/v$  and a relative time shift  $d\tau/\tau$  between the reference and the current CF. Assuming  $dv/v$  homogeneous in space, one can demonstrate that (Ratdomopurbo and Poupinet; 1995):

$$\frac{dv}{v} = -\frac{d\tau}{\tau} \quad (1)$$

Under this assumption, the relative velocity variation  $dv/v$  is simply obtained by estimating the relative travel time shift between the reference CF and the current CF.

We tested two different methods to evaluate  $dv/v$ , and compare their results in quasi real-time routines: the MWCSA and the stretching technique (detailed in Appendix). In both cases,  $dv/v$  is estimated using the CF part corresponding to the scattered wavefield with typical lags ranging from 5 and 20 s.

## 3. Results

The analysis described above is implemented since late 2006. It allows to follow the relative velocity variations associated with the 2007 collapse in quasi real time, since each value of  $dv/v$  represents the velocity variation over the last 10 days compared to the long term averaged value. The period of investigation was extended back to January 2006 in order to compare different eruptions' responses over the whole 2006–2007 eruptive cycle. The reference CF should be computed over a quiet period without eruption or cyclone. For year 2006, we selected the April to July period to compute the reference CF and the January to March 2007 period for the reference CF of the year 2007. In order to obtain the relative velocity variations over the whole period,  $dv/v$  was estimated between the two reference CF using the two methods (see examples in Table 1). For the sake of clarity, eruptions are named by the month of

**Table 1**

Examples of  $dv/v$  estimated between the two reference CF using the MWCSA and the stretching technique.

Station pair	Time window	$dv/v$ MWCSA	$dv/v$ stretching
bor-fer	5 s–25 s	$0.51\% \pm 0.13\%$	$0.65\% \pm 0.11\%$
fer-dsr	5 s–25 s	$0.34\% \pm 0.09\%$	$0.44\% \pm 0.12\%$
SFR-ferz	5 s–20 s	$0.41\% \pm 0.17\%$	$0.66\% \pm 0.10\%$
TCR-bor	5 s–25 s	$0.01\% \pm 0.02\%$	$-0.06\% \pm 0.07\%$
TCR-dsr	5 s–20 s	$0.24\% \pm 0.05\%$	$0.23\% \pm 0.04\%$
TCRZ-ferz	8 s–25 s	$0.58\% \pm 0.03\%$	$0.54\% \pm 0.05\%$

For each pair of stations, we specify in which time window  $dv/v$  have been computed.

**Table 2**  
Eruptions at the Piton de la Fournaise volcano from December 2005 to June 2007.

Date	Seismic-crisis	Altitude (m)	bf eruption duration	Type
Dec 26, 2005	130 min	1800	23 days	Distal
July 20, 2006	102 min	2200	25 days	Lateral
Aug 30, 2006	–	2500	124 days	Summital
Feb 18, 2007	27 min	2500	9 h	Summital
March 30, 2007	144 min	1880	9 h	Lateral
April 2, 2007	2760 min	575	29 days	Distal

their onset (for example, the eruption that begins on August 30, 2006 is named “the August 2006 eruption”; see Table 2).

3.1. Linear evolution of the time shift between two stations

Details of the time shift observed between the reference CF and the “current” CF 10 days before the July 2006 eruption started are shown in Fig. 3A–B. As expected, the CF at early times corresponding to

ballistic waves, doesn't seem to be affected by temporal variations whereas the later arrivals corresponding to the scattered waves, are clearly shifted (Fig. 3A,B).

The evolution of  $d\tau$  along the CF (Fig. 3D) shows a linear trend as described in Eq. (1). Such temporal variations are especially marked for stations close to each other and located at the PdF summit. It is not necessarily the case for increasing distances between stations or for stations located outside of the Enclos Fouqué caldera suggesting that the relative velocity variations have a limited spatial extension.

3.2. Temporal variations time series

Fig. 5A–B shows the relative velocity changes for station pair “fer-dsr” from January 2006 to June 2007 using both methods. Another example of  $dv/v$  variations estimated for station pair “bor-fer” with the stretching technique is shown on Fig. 6A. The gaps correspond to low quality measurements (i.e. when error on the  $dv/v$  estimate exceed 1%): the GF was not well recovered along these periods, due to either high seismicity, important tremor sources during eruptions,

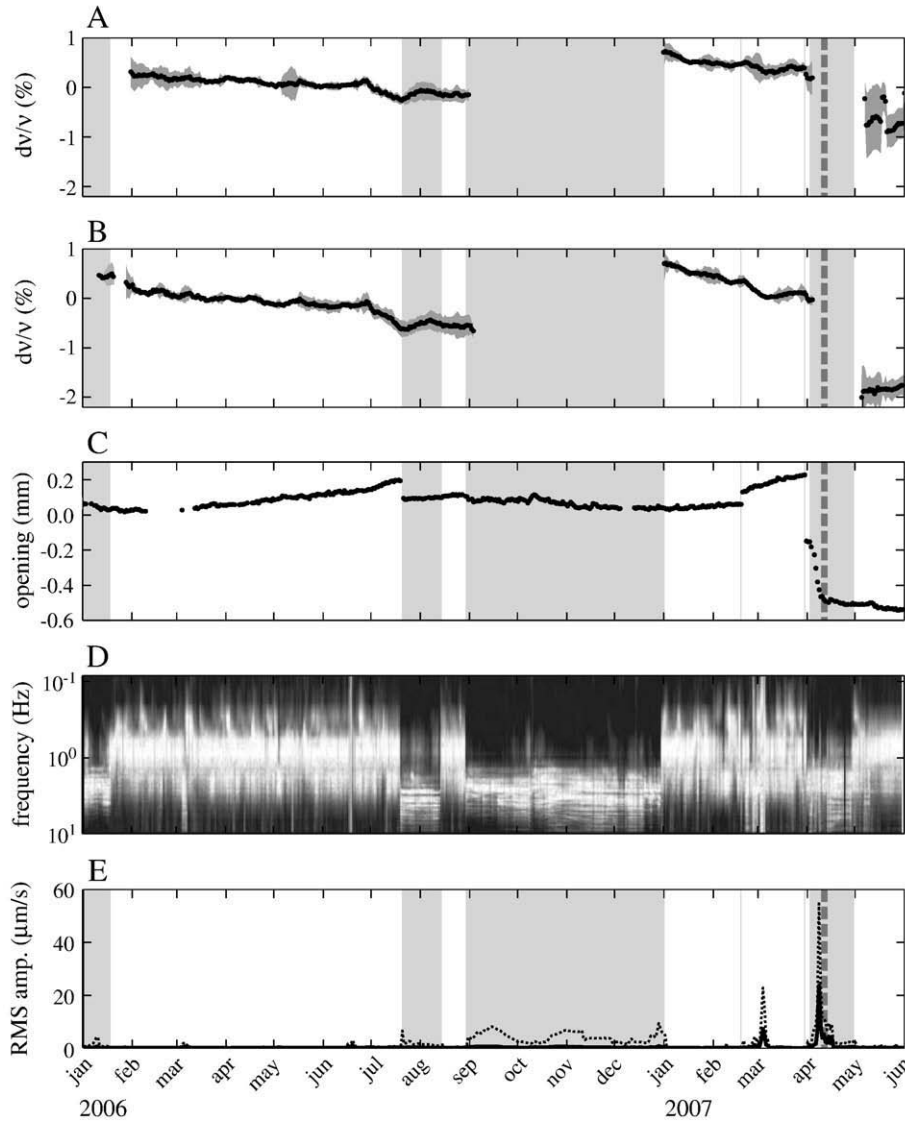


**Fig. 5.** Comparison between surface fracture aperture and relative velocity variations for station pair “fer-dsr” using the MWCA and the stretching technique. Dark grey areas represent periods of eruption. The vertical dotted dark grey line in April 2007 delimits the collapse in the Dolomieu crater. (A), Temporal changes inferred from MWCSA. (B), Variation in seismic velocities deduced from the stretching technique. Error bar associated to each methods are in light grey. The  $dv/v$  values are placed at the end of the ten day windows used to compute the current CF. (C), Extensometer displacements recorded on the opening component at “CHAF” (Fig. 1). (D), Spectrogram for station “bor” based on the normalized spectral amplitude of a one minute moving window. (E) Daily RMS amplitude computed at station “bor” (plain line) between 0.5 and 1 Hz and (dotted line) between 1.5 and 7 Hz.

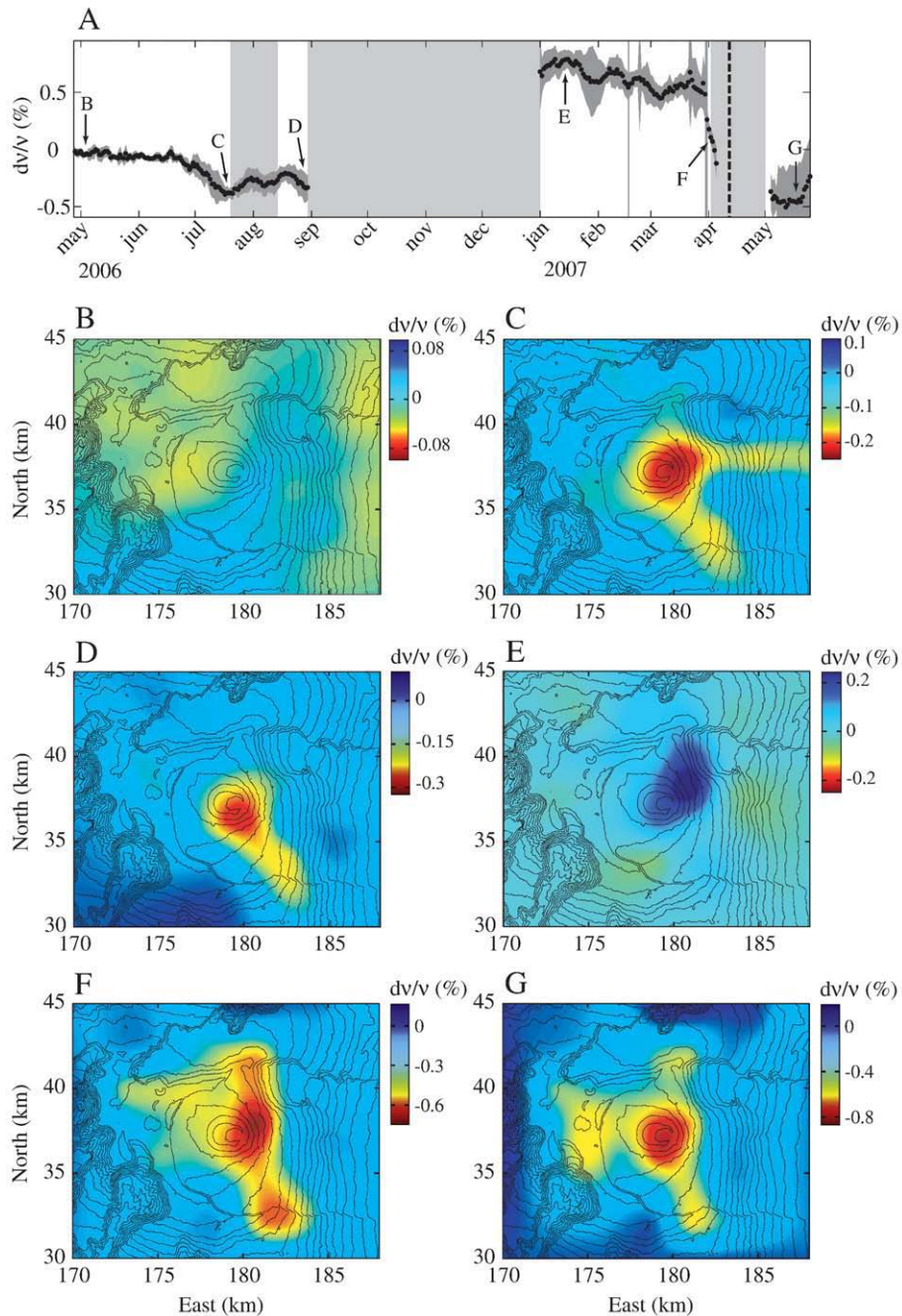


**Fig. 6.** Regionalization of temporal changes for 2006 and 2007. The  $dv/v$  values are obtained using the stretching technique described in the Appendix. (A), Variation in seismic velocity for the pair bor–fer. The period taken for regionalisation maps showed are specified with the arrows and the corresponding letters: (B), period without eruption or cyclones. (C), July 2006 pre-eruptive period. (D), August 2006 pre-eruptive phase. (E), August 2006 post-eruptive period. (F), March–April 2007 inter-eruptive period. (G), Variation after the July 2006 eruption and the Dolomieu collapse.

noise perturbation during the cyclonic season, thunderstorm, or damaged instruments.

The following marked changes in  $dv/v$  are observed on Figs. 5A–B and 6A:

- (1)  $dv/v$  decreases of about 0.3% 10 days before the beginning of the July 2006 eruption and remains quite stable until the onset of the August 2006 eruption.
- (2) During the August 2006 eruption the velocity increases since  $dv/v \approx +0.2\%$  on July 30, 2006 and  $dv/v \approx -0.6\%$  on January 10, 2007.
- (3) From January to the onset of the February eruption  $dv/v$  seems to decrease.

- (4) Between the February 2007 eruption and the onset of the March 2007 eruption  $dv/v$  slightly decreases.
- (5) Following the March 2007 eruption,  $dv/v$  decreases again until April 5.
- (6) At the end of the April 2007 eruption,  $dv/v$  remains at a relatively low value suggesting a strong velocity decrease during the eruption.

On Fig. 5C, these variations are compared with the opening component of the extensometer “CHAF” located on the PdF south flank (Fig. 1). The short term variations shown in Fig. 5C at the onsets of the July 2006, February 2007 and March 2007 eruptions should not be interpreted as a global evolution over the PdF. These sudden

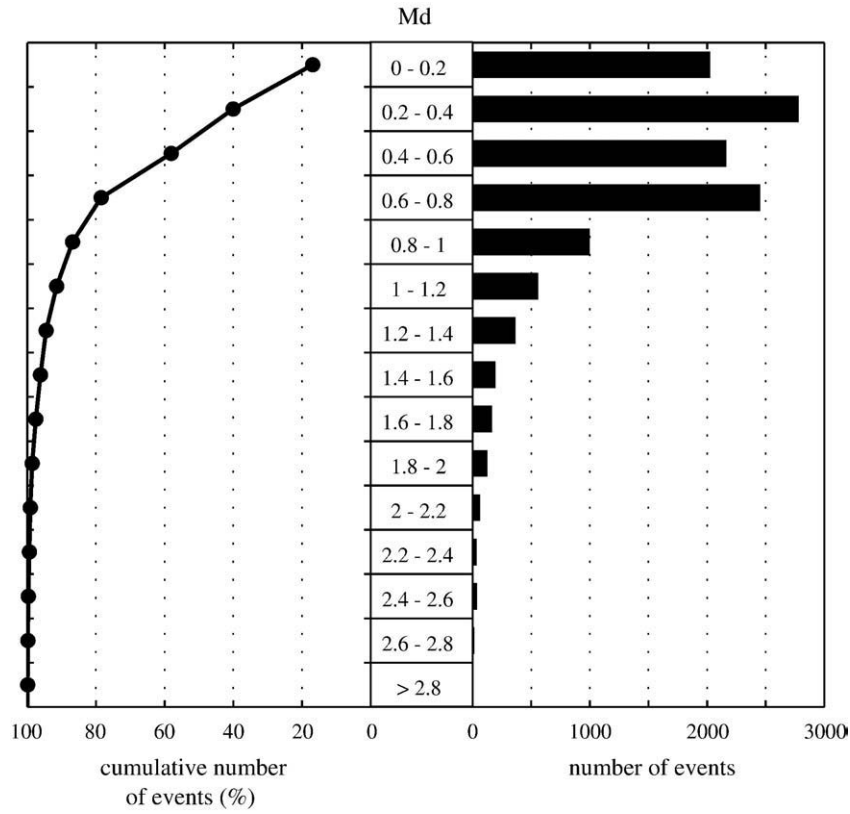


Fig. 7. Duration magnitudes ( $M_d$ ) of volcano tectonic events from January 2006 to June 2007 versus (right) the number of events and (left) the cumulative percentage of events.

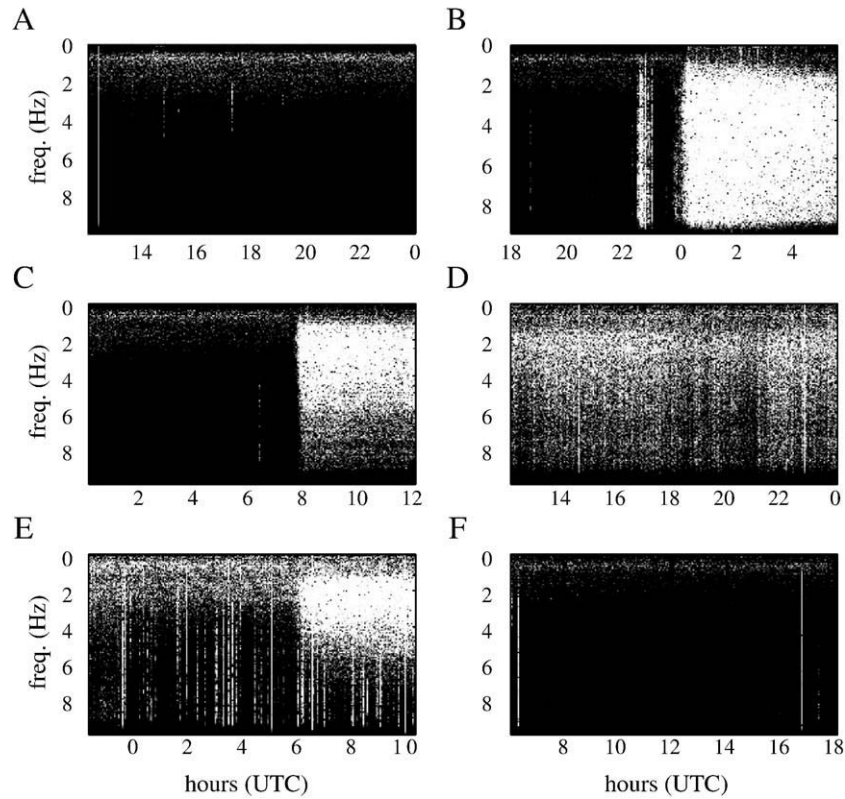
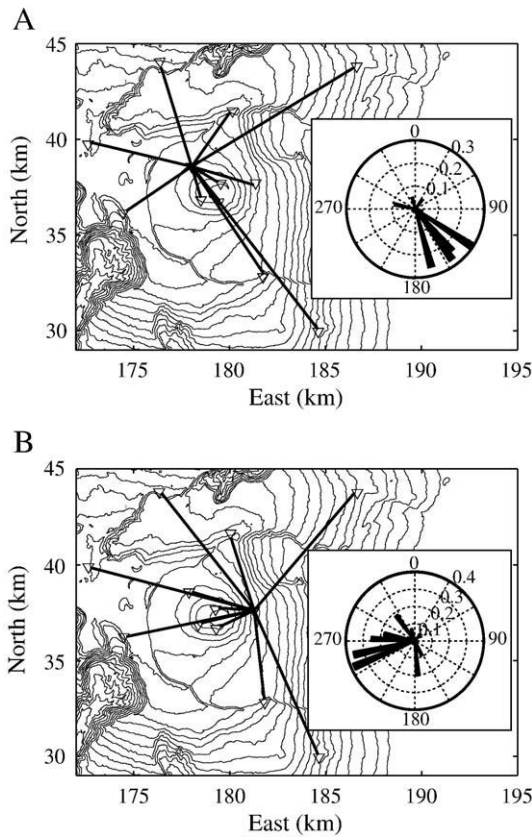


Fig. 8. Detailed spectrograms for station “bor”. We compute the spectral amplitude using a one minute moving window. The linear color scale is from 0 to  $20 \mu m^{-1}$ . Twelve hours of signal are shown from (A), May 7, 2006 at 12 h UTC (B), July 20, 2006 at 18 h UTC (C), August 30, 2006 at 0 h UTC (D), February 26, 2007 at 12 h UTC (E), April 2, 2007 at 22 h UTC (F), May 28, 2007 at 6 h UTC. Since earthquakes correspond to a large frequency bandwidth, we will easily recognise seismic events by vertical white lines from low frequency until 10 Hz.



**Fig. 9.** Distribution of absolute relative velocity changes as a function of azimuth for stations pairs containing TCR or fer. The “current” cross-correlation function is averaged over the 10 days before the July 2006 eruption starts. The  $dv/v$  values are obtained using the stretching technique described in the Appendix. (A) TCR attached pairs. (B) fer attached pairs.

deformations are clearly a near field effect due to the opening of eruptive fissures close to the extensometer. One should rather work on the more representative long-term variations.

Reconstruction of the GF from seismic noise is based upon the critical assumption of a randomly scattered wavefield, i.e. a wavefield generated by a spatially homogeneous distribution of seismic sources. This assumption fails if the radiation from a single, spatially localized source dominates over the stochastic components of the wavefield. In order to assess the effects of the seismicity and eruption tremor on our measurements, Fig. 5D shows a spectrogram and Fig. 5E displays the daily averaged amplitude (RMS amplitude) computed for station “bor” over the whole period of analysis.

During quiet periods, Fig. 5D shows a dominant low frequency signal (below 1 Hz) corresponding to microseismic noise. Fig. 5E shows that these periods correspond to low signal amplitude in the frequency band 0.5 to 1 Hz and 1.5 to 7 Hz. As seen on Fig. 5D–E, the eruption tremor is characterized by a dominant frequency ranging from 2 to 5 Hz and different RMS amplitudes depending on the eruption location, site, intensity and distance from the station. It can be seen on Fig. 5E that most of the seismic energy released during an eruption corresponds to frequencies higher than 1.5 Hz. For the analyzed period, the tremor disappears completely when the surface activity stops.

Fig. 7, displays the duration magnitude of earthquakes observed at the PdF in 2006 and 2007. For small events, the distribution of magnitudes is quite undervalued due to earthquake detection limits in the background noise. Moreover, duration magnitudes were not sampled properly during the seismic crisis that preceded the Dolomieu crater collapse during the April 2007 eruption. Because of the quasi-continuous seismic activity, earthquakes were continuously

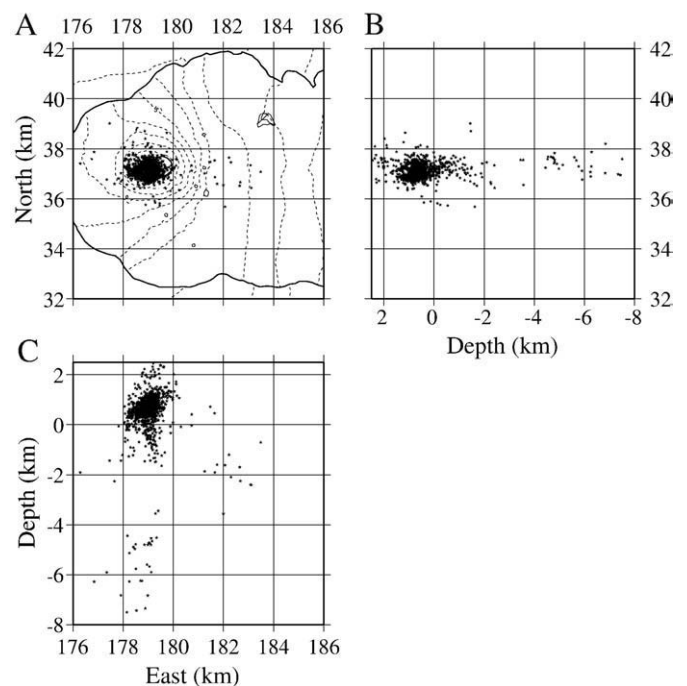
overlapping each other, preventing us from determining their durations using classical picking methods. However, it is clear that seismic events observed at the PdF are very small compared to those encountered at other volcanoes. From the 9472 earthquakes counted in 2006/2007, the magnitudes rarely exceed  $M_d=2$  and 90% of the events have a magnitude lower than 1, which corresponds to a duration shorter than 10 s.

At the PdF, inter-eruptions periods are marked by low seismicity (0 to 3 earthquakes with  $M_d<0.5$  per day) as can be seen on Figs. 5D, 8A and F. Intense seismic crisis are characteristic of magma intrusion and may last from a few minutes to a few days until the eruption starts, usually depending on the elevation of the eruptive fissure (see spectrograms on Fig. 8B and E and seismic crisis durations on Table 2).

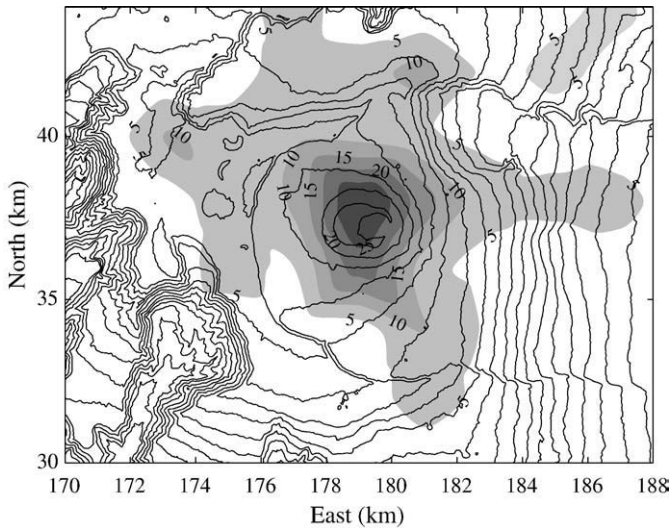
### 3.3. Location of relative velocity changes in the propagating medium

Fig. 9A and B displays the relative velocity changes averaged 10 days before the July 2006 eruption started between station “TCR” (A) and “fer” (B) and all of the other stations. They reveal a clear dependency of  $|dv/v|$  with the azimuth, suggesting that the velocity variations mostly affect the central cone of the PdF. This is consistent with data from GPS, extensometer and tiltmeter networks, all of them showing a deformation of the central cone during pre- or post-eruptive periods (Peltier, 2007). Earthquakes are also strongly localized beneath the Bory and Dolomieu craters above sea level (Fig. 10). Thus, eruption-induced changes of the edifice elastic properties can be assumed to be mostly located in the central cone.

To represent the location of the corresponding velocity changes while taking into account the whole set of seismic stations, we apply a regionalization procedure as described by Brenguier et al. (2008). Once  $dv/v$  is estimated for each pair of stations, the obtained values are averaged in  $2 \times 2$  km cells around the direct Ray path. These values are then interpolated in the facets of the Delaunay triangulation based on the cells center points. del at  $x=157$  and  $200$  km,  $y=21$  and  $51$  km in Gauss Laborde coordinates (Fig. 1).



**Fig. 10.** Hypocentral locations during the period from January 2006 to June 2007. We selected the events of quality A and B resulting from the inversion program “HYPO71” (Lee and Lahr, 1972). Map view (A) and projection on (B) N–S section and (C) E–W section are presented.



**Fig. 11.** Contour map of the coverage used for the regionalisation procedure. It corresponds to the number of direct paths passing by cells of  $2 \times 2$  km.

The spatial resolution of the regionalization is highly dependent on the coverage defined by direct paths between station pairs and is best defined over the central cone as shown in Fig. 11. Since the coda corresponds to waves multiply scattered over a large volume, this method results should not be considered as a completely realistic image of the changes spatial distribution. They help to visualize which station pairs are affected by  $dv/v$  variations but should not be interpreted as tomographic images resulting from a proper inversion.

The velocity changes regionalization maps obtained at different times between May 2006 and June 2007 are presented in Fig. 6. They depict significant temporal variations with varying velocities mostly affecting the central cone and will be discussed in the next section.

#### 4. Discussion

At the PdF, Peltier (2007) distinguishes three types of eruptions that differ mainly by their location relative to the central cone: summital eruptions take place in the main craters (Bory and Dolomieu), lateral or proximal eruptions are located on the central cone flanks and distal eruptions occur at lower altitude and away from the cone. From January to June 2007, 5 eruptions (listed in Table 2) occurred, showing a great diversity of characteristics, such as the fissure location, the eruption duration, the intensity and the volume of emitted lava. This period of activity started with the July and August 2006 proximal eruption and ended with the major distal eruption of April 2007 during which the entire Dolomieu crater collapsed.

##### 4.1. The July 2006, August 2006 and February 2007 eruptions

Comparing Fig. 5A and B from January 2006 to the end of February 2007,  $dv/v$  estimates do not seem to depend on the method used. However, it can be noted that the stretching technique involves slightly larger relative velocity variations than those obtained with the MWCSA.

The July 2006 eruption is preceded by a velocity drop of about 0.3% (Figs. 5A–B and 6A, see (1) in Section 2). The value of  $dv/v$  then remains quite stable until the onset of the August 2006 eruption. On Fig. 6C–D, we notice that station pairs located on the eastern part of the central cone are mostly affected.

Fig. 5D–E shows a low seismic activity before the July 2006 eruption. As can be seen on Fig. 8B, this eruption was only preceded by a small seismic crisis at 22h20 UTC, 102 min before the tremor started (see Table 2). This seismic tremor is relatively low as indicated by the

RMS amplitudes on Fig. 5E, suggesting that the July 2006 eruption has a little effect on our measurements. However, on Fig. 5A the error in  $dv/v$  estimates slightly increases while a little gain in velocity is observed: this could be a consequence of the sources localization on the eruptive vent. The inter-eruptive period that follows the July 2006 eruption is characterized by low seismic activity (Fig. 5D–E) and the August 2006 eruption was not preceded by a seismic crisis (Fig. 8C and Table 2).

Knowing the spectral and temporal normalizations involved in data processing and the low seismicity observed on PdF during this period, it is clear that earthquakes have a negligible influence on the relative velocity variations obtained 10 days before the July 2006 eruption begins. Furthermore, even if a little perturbation of  $dv/v$  measurements is observed after the beginning of the tremor, the velocity anomaly remains quite stable until the August 2006 eruption whereas the seismicity stops with the onset of the July 2006 eruption.

The velocity decrease that precedes the July 2006 eruption could reflect the dilatation of the propagation medium due to the tensile stresses induced by over-pressurization of the magma reservoir and subsequent magma migration towards the surface (Patanè et al., 2006; Brenguier et al., 2008). Such increases of the tensile stresses above a pressuring magma chamber have been theoretically predicted by Pinel and Jaupart (2003). Fracture opening during the pre-eruptive stages was also measured by the extensometers, while GPS and tiltmeter networks revealed an inflation of the central cone accompanying the velocity drop (Fig. 12A).

Figs. 5A–B and 6A show an increase of the seismic velocity during the August 2006 eruption (see (2) in Section 2). Despite the lack of measurements due to the eruption tremor at the center of the seismic network (Fig. 5E), this period corresponds to a significant increase in seismic velocity. This is confirmed by positive values of  $dv/v$  measured between reference CFs averaged from April to July 2006 and from January to March 2007 (Table 1). The same relative velocity variation is obtained by calculating  $dv/v$  between the reference CF averaged in 2006 and the current CFs averaged over 10 days at the beginning of

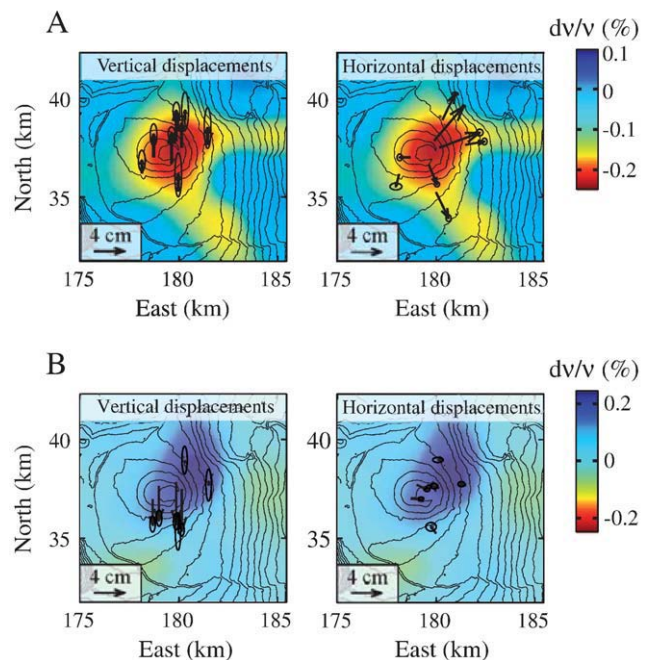


**Fig. 12.** Comparison between velocity changes and deformations revealed by the GPS permanent network (Peltier et al., 2009-this issue).  $dv/v$  regionalisations correspond to Fig. 6C and E. (left) Vertical and (right) horizontal displacements are shown (A), during the pre-eruptive inflation between the 23rd of March and the 20th of July 2006 (B), during the deflation from the 31st of August until the 31st of December 2006.

year 2007. Finally, the lack of seismicity during January 2007 also validates our measurements at this time.

Such an increase in seismic velocities could be interpreted as the reverse of the process described above, i.e. the apparition of compressive horizontal stress with the magma chamber depressurization due to the large quantity of extruded magma. Fracture closure of about 0.1 mm was also observed at “CHAF” (Fig. 5C) and a summit deflation was revealed by GPS and tiltmeter networks. From the August 31 to December 31, 2006, vertical displacements of the order of  $-4$  cm were observed at GPS stations located on the summit area (Fig. 12B). This deflation could be emphasized by a loading exerted by the important lava accumulation on the Dolomieu crater floor, reaching a volume of 20 million  $\text{mm}^3$ .

As seen for the July 2006 eruption, it can be noticed on Fig. 6E that the velocity changes associated with the August 2006 eruption mostly affects station pairs located on the Eastern part of the central cone. Fig. 12 shows that the deformation is in accordance with these regionalization images. The east flank is mostly affected by the horizontal displacements during the July 2006 pre-eruptive inflation and by vertical displacements after the August 2006 eruption. We could associate this localised perturbation as an effect of the east flank instability induced by the presence of rift zones (Letourneur et al., 2008).

It can be seen on Figs. 5 and 6A, that the inter-eruptive period from January to February 2007 did not show a clear velocity drop before the February 2007 eruption (see (3) in Section 2). This may be due magma ascension following pre-existent paths associated with the July and the August 2006 eruptions.

Between the February eruption and the beginning of March 2007 a velocity decrease can be observed on Fig. 5B (see (4) in Section 2). However, on Figs. 5A and 6A, large error bounds accompanied this variation which is followed by a quick increase of  $dv/v$ , retrieving its initial value at mid-February 2007. Figs. 5D and 8D show a modification of the signal frequency content during that period, while Fig. 5E displays a sudden increase of the daily RMS amplitude between 1.5 Hz and 7 Hz but also in the 0.5–1 Hz frequency band in  $dv/v$  estimates from the end of February until the beginning of March 2007. This is clearly related to the Cyclone Gamède passage on La Réunion Island at this period. Heavy rainfall and winds probably generate high frequencies whereas low frequency signal may be generated by cyclonic swells that encounter the coastline.

#### 4.2. Velocity variations associated with the caldera collapse of April 5, 2007

The period from March 30, to April 5, 2007, seems to be associated with a decrease in the subsurface velocity as shown on Figs. 5A–B and 6A (see (5) in Section 2). However, the anomaly presented on Fig. 6F shows a marked trend towards the south; this suggests that the tremor of the March 2007 eruption influenced on our measurements, since the CF are averaged over 10 days. An important seismic activity can also be observed, starting from March 30, as shown by the spectrograms on Figs. 5D and 8E and reported in Table 2. Until the Dolomieu collapse, the seismicity intensification and the volcanic tremor growing are revealed by a rapid increase of the daily RMS amplitudes in both frequency bands 0.5–1 Hz and 1.5–7 Hz (Fig. 5E). Therefore, the observed decrease in  $dv/v$  could be an artefact of the CF perturbation and may not reflect a velocity decrease in the propagation medium.

Be that as it may,  $dv/v$  values observed after the April 2007 eruption suggest a strong velocity decrease during the eruption (see (6) in Section 2). This important velocity change concerns mostly the seismic stations located around the Dolomieu crater (Fig. 6G). The post-eruptive period is relatively quiescent as can be seen on Figs. 5D–E and 8E and the observed  $dv/v$  variation can't be an artefact due to seismicity, tremor or bad weather conditions.

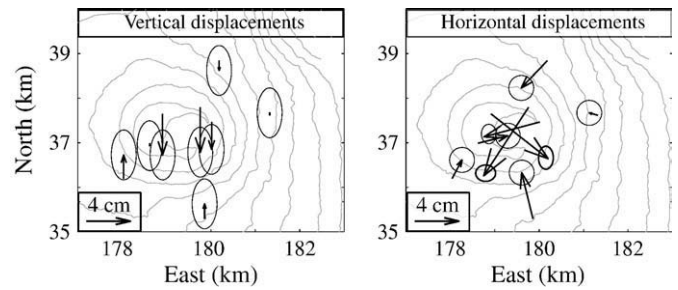


Fig. 13. Deflation during the April 2007 eruption until the Dolomieu collapse onset, i.e. from the 2nd to the 5th of April. (Peltier et al., 2009-this issue). (left) Vertical and (right) horizontal displacements are presented.

On Fig. 5, after the April 2007 eruption, the MWCSA shows a dispersion of the measured  $dv/v$  around 0.7% while the stretching technique appears to be more stable with  $dv/v \approx 1.7\%$ . This instability is inherent to the MWCSA that uses several small time windows in which  $d\tau$  is supposed constant. This technique seems to work very well for small  $d\tau/\tau$  and for  $d\tau$  that are small relative to the dominant wavelength, but becomes unstable for large values of  $d\tau/\tau$ . If  $d\tau/\tau$  is important,  $d\tau$  increases rapidly with  $\tau$  and we risk to correlate the wrong wave cycles together. On the other hand, the stretching technique appears to be more stable at this time because it involves a unique large window in which the model specified in Eq. (1) is assumed.

From the onset of the April 2007 eruption, Fig. 5C shows a fracture closure at “CHAF” and a deflation of the central cone is revealed by the GPS network (Fig. 13). The velocity drop associated with the April 2007 eruption may involve a different process than for eruptions occurring without edifice destruction. This strong decrease in  $dv/v$  may be interpreted as a combined result of the failure of the rock column and the subsurface perturbation due to the vacuum created by the entire Dolomieu crater collapse to a depth of 350 m during the April 2007 eruption.

## 5. Conclusion

We demonstrated the suitability of coda-wave interferometry from seismic noise for the real-time monitoring of relative velocity changes of less than 1% in a volcanic context. This confirms the existence of reflected and scattered waves in the GF that can be retrieved from the correlation of seismic noise between two stations. For each possible receiver pair, we assume a spatially homogeneous relative velocity perturbation that supposes a linear evolution of the temporal variation  $d\tau/\tau$  as a function of time. We tested 2 methods for determining the relative velocity variation; the results were quite similar except for the April 2007 eruption where the stretching technique appeared to be much stable.

Resulting velocity changes appear to be correlated with the volcano-tectonic activity at the PdF. The seismic velocity variations observed on PdF from January 2006 to March 2007 are consistent with the analytical elastic models exposed in the literature (Pinel and Jaupart, 2003). During this period, we interpreted the relative velocity changes as an effect of the edifice dilatation or compression due to the chamber pressure variations. The regionalization method used reveals that these velocity changes mostly affect stations located on the central cone. This is in agreement with the measurements of GPS, tiltmeter and extensometer networks. The April 2007 eruption shows a different behavior with an important velocity drop that may be linked to the intense fracturation of the rock column above the magma chamber with a possible influence of the void created by the collapse affecting the entire Dolomieu crater. Thus, a deflation of the summit cone as observed by GPS network,

may be associated either to an increase or to a decrease of the velocity depending on the state of the subsurface.

The method depends upon the quality and the density of the network and we still consider that the relative velocity variation is homogeneous between each station pairs. For a precise localization, it would be necessary to turn our attention on the approach done by Pacheco and Snieder (2005). However, it would require a very dense network and the complexity of the involved processes may still be an obstacle. Increasing the density of seismic stations inside the Enclos Fouqué caldera would allow us to overcome these difficulties but it is clear that such high density networks are impossible to maintain permanently on most volcanoes in the world. Anyhow, coda-wave interferometry from seismic noise cross-correlation functions appears to be a promising tool that can be set up on active volcanoes because of the simplicity of its implementation and its potential capacity to forecast eruptions even with a limited number of stations.

### Acknowledgments

All data used in this work was collected by the network of the Observatoire Volcanologique du Piton de la Fournaise. We are grateful to the Observatory staff for the help with data acquisition. We thank Sheldon Warden, Frederick Massin and Aline Peltier for their careful reading of the manuscript. We are grateful to Luis Rivera and Gerard Wittlinger, without their support this would not have been possible. This is IGP contribution no 2452.

### Appendix A. The MWCSA and the stretching technique

The “moving window cross spectral analysis” (MWCSA) consists in measuring travel time shifts ( $d\tau_i$ ) at different times  $\tau_i$  (Poupinet et al., 1984; Ratdomopurbo and Poupinet, 1995; Snieder et al., 2002). The cross-correlation is computed between the current CF and the reference CF. This evaluation is made in independent time windows centered at lag  $\tau_i$  in the causal and anticausal part. As we consider that  $d\tau_i$  evolves linearly with  $\tau_i$  along the CF, a linear regression passing through zero allows to estimate  $dv/v$ . The error on the  $dv/v$  estimation is calculated as:

$$E_{dv/v} = \sqrt{\frac{\sigma_{d\tau}}{\sum_{i=1}^N \tau_i^2}} \quad (2)$$

with  $\sigma_{d\tau}$  the fitting residual:

$$\sigma_{d\tau} = \frac{\sum_{i=1}^N (d\tau_i + dv/v \times \tau_i)^2}{N} \quad (3)$$

The “stretching technique” consists in stretching or compressing the reference CF in order to obtain the best coherency with the current CF (Sens-Schönfelder and Wegler, 2006). Before inversion, the causal and anticausal part of the CF are averaged. Considering an homogeneous  $dv/v$  as described in Eq. (1), one can compute the corresponding time-shifted correlation  $S(\tau)$  from the reference one  $R(\tau)$ :

$$S(\tau) = R(\tau(1 + dv/v)) \quad (4)$$

Because we work on discrete signals, the shifted amplitude  $S_i$  at a given time  $\tau_i$  is deduced from a linear interpolation at time  $\tau_i(1 + dv/v)$  between sample amplitudes  $R_j$  and  $R_{j+1}$  on the reference CF:

$$S_i = R_j + \frac{R_{j+1} - R_j}{dt} [\tau_i(1 + dv/v) - \tau_j] \quad (5)$$

Here,  $dt$  denotes the sampling period and  $\tau_j$  is the lag corresponding to  $R_j$ . Knowing the sampling rate used ( $dt = 0.01$  s), we choose to compute 5000 trials for  $dv/v$  ranging in the interval  $(-0.03; 0.03)$ . Finally, we select the trial that corresponds to the highest correlation coefficient between the shifted CF and the current CF. In order to

assess the quality of our measurements using this method, we estimate a standard deviation by estimating  $(dv/v)_i$  in different time windows ( $i = 1, N$ ):

$$E'_{dv/v} = \sqrt{\frac{\sum_{i=1}^N [(dv/v)_i - dv/v]^2}{N}} \quad (6)$$

### References

- Aki, K., 1985. Theory of earthquake prediction with special reference to monitoring of the quality factor of lithosphere by the coda method. *Earthq. Predict. Res.* 3, 219–230.
- Aki, K., Ferrazzini, V., 2000. Seismic monitoring and modeling of an active volcano for prediction. *J. Geophys. Res.* 105, 16617–16640.
- Aki, K., Richards, P.G., 2002. *Quantitative Seismology*, 2nd Edition. University Science Books, 700 pp.
- Brenguier, F., Shapiro, N.M., Campillo, M., Nercessian, A., Ferrazzini, V., 2007. 3-D surface wave tomography of the Piton de la Fournaise volcano using seismic noise correlations. *Geophys. Res. Lett.* 34 (2), L02305. doi:10.1029/2006GL028586.
- Brenguier, F., Shapiro, N.M., Campillo, M., Ferrazzini, V., Duputel, Z., Coutant, O., Nercessian, A., 2008. Toward forecasting volcanic eruptions using seismic noise. *Nat. Geosci.* doi:10.1038/ngeo104.
- Grêt, A., Snieder, R., Aster, R.C., Kyle, P.R., 2005. Monitoring rapid temporal changes in a volcano with coda wave interferometry. *Geophys. Res. Lett.* 32, L06304. doi:10.1029/2004GL021143.
- Goldstein, P., Dodge, D., Firpo, M., Ruppert, L., 1998. What's new in SAC2000? Enhanced processing and database access. *Seismol. Res. Lett.* 69, 202–205.
- Jin, A., Aki, K., 1986. Temporal change in coda Q before the Tangshan earthquake of 1976 and the Haicheng earthquake of 1975. *J. Geophys. Res.* 91, 665–674.
- Johnson, C.E., Bittenbinder, A., Bogaert, B., Dietz, L., Kohler, W., 1995. Earthworm: a flexible approach to seismic network processing. *IRIS Newsletter* 14, 1–4.
- Lee, W.H.K., Lahr, J.C., 1972. HYP071: A computer program for determining hypocenter, magnitude, and first motion pattern of local earthquakes. U. S. Geological survey Open File Report, p. 80-59, 59 pp.
- Letourneur, L., Peltier, A., Staudacher, T., Gudmundsson, A., 2008. The effects of rock heterogeneities on dyke paths and asymmetric ground deformation: the example of Piton de la Fournaise (Réunion Island). *J. Volcanol. Geotherm. Res.* 173, 289–302. doi:10.1016/j.jvolgeores.2008.01.018.
- Nercessian, A., Hirn, A., Lépine, J.C., Sapin, M., 1996. Internal Structure of Piton de la Fournaise volcano from seismic wave propagation and earthquake distribution. *J. Volcanol. Geotherm. Res.* 70 (3–4), 123–143.
- Pacheco, C., Snieder, R., 2005. Time-lapse travel time change of multiply scattered acoustic waves. *J. Acoust. Soc. Am.* 118, 1300–1310.
- Patanè, D., Barberi, G., Cocina, O., De Gori, P., Chiarabba, C., 2006. Time-resolved seismic tomography detects magma intrusions at Mount Etna. *Science* 313 (5788), 821–823. doi:10.1126/science.1127724.
- Peltier, A., 2007. Suivi, modélisation et évolution des processus d'injections magmatiques au Piton de La Fournaise (La Réunion). PhD thesis in French, Géosciences Réunion.
- Peltier, A., Staudacher, Th., Catherine, Ph., Ricard, L., Kowalski, Ph., Bachelery, P., 2006. Subtle precursors of volcanic eruptions at Piton de la Fournaise detected by extensometers. *Geophys. Res. Lett.* 33 (6), L06315.1–L06315.5. doi:10.1029/2005GL025495.
- Peltier, A., Staudacher, Th., Bachelery, P., Cayol, V., 2009. Formation of the April 2007 caldera collapse at Piton de La Fournaise volcano: Insights from GPS data. *J. Volcanol. Geotherm. Res.* 184, 152–163 (this issue). doi:10.1016/j.jvolgeores.2008.09.009.
- Pinel, V., Jaupart, C., 2003. Magma chamber behavior beneath a volcanic edifice. *J. Geophys. Res.* 108 (B2), 2072. doi:10.1029/2002JB001751.
- Poupinet, G., Ellsworth, W.L., Frechet, J., 1984. Monitoring velocity variations in the crust using earthquake doublets: an application to the Calaveras Fault, California. *J. Geophys. Res.* 89, 5719–5731.
- Ratdomopurbo, A., Poupinet, G., 1995. Monitoring a temporal change of seismic velocity in a volcano: application to the 1992 eruption of Mt. Merapi (Indonesia). *Geophys. Res. Lett.* 22 (7), 775–778.
- Roux, P., Sabra, K.G., Gerstoft, P., Kuperman, W.A., Fehler, M.C., 2005. P-waves from cross-correlation of seismic noise. *Geophys. Res. Lett.* 32, L19303. doi:10.1029/2005GL023803.
- Sabra, K.G., Gerstoft, P., Roux, P., Kuperman, W.A., Fehler, M.C., 2005. Extracting time-domain Green's function estimates from ambient seismic noise. *Geophys. Res. Lett.* 32, L03310. doi:10.1029/2004GL021862.
- Sato, H., Fehler, M.C., 1998. *Seismic wave propagation and Scattering in the Heterogeneous Earth*. Springer-Verlag, New York, 308 pp.
- Sens-Schönfelder, C., Wegler, U., 2006. Passive image interferometry and seasonal variations of seismic velocities at Merapi volcano, Indonesia. *Geophys. Res. Lett.* 33, L21302. doi:10.1029/2006GL027797.
- Shapiro, N.M., Campillo, M., 2004. Emergence of broadband Rayleigh waves from correlations of the ambient seismic noise. *Geophys. Res. Lett.* 31, L07614. doi:10.1029/2004GL019491.
- Snieder, R., 2006. The theory of coda wave interferometry. *Pure Appl. Geophys.* 163, 455–473.
- Snieder, R., Grêt, A., Scales, J., 2002. Coda wave interferometry for estimating nonlinear behavior in seismic velocity. *Science* 295 (5563), 2253–2255. doi:10.1126/science.1070015.
- Stehly, L., Campillo, M., Shapiro, N.M., 2006. A study of the seismic noise from its long range correlation properties. *J. Geophys. Res.* 111, B10306. doi:10.1029/2005JB004237.
- Wegler, U., Sens-Schönfelder, C., 2007. Fault zone monitoring with passive image interferometry. *Geophys. J. Int.* 168, 1029–1033.